Rezazadeh et al., *BioImpacts.* 2024;14(6):30159
doi: 10.34172/bi.2024.30159
https://bi.tbzmed.ac.ir/

Synthesis and characterization of a magnetic bacterial cellulose-chitosan nanocomposite and evaluation of its applicability for osteogenesis

Nahid Rezazadeh[1], Effat Alizadeh[2], Somaieh Soltani[3], Soodabeh Davaran[3,4*], Neda Esfandiari[1*]

[1]Faculty of Life Sciences and Biotechnology, Shahid Beheshti University, Tehran, Iran
[2]Department of Medical Biotechnology, Faculty of Advanced Medical Sciences, Tabriz University of Medical Sciences, Tabriz, Iran
[3]Drug Applied Research Center, Tabriz University of Medical Science, Tabriz, Iran
[4]Department of Toxicology, Faculty of Pharmacy, Yeditepe University, Istanbul, Turkey

Article Info

Article Type:
Original Article

Article History:
Received: 17 Oct. 2023
Revised: 6 Jan. 2024
Accepted: 9 Jan. 2024
ePublished: 24 Mar. 2024

Keywords:
Bacterial cellulose,
Chitosan,
Magnetic Fe_3O_4 nanoparticles,
Biocompatible scaffold,
Natural polymers,
Osteogenic differentiation

Abstract

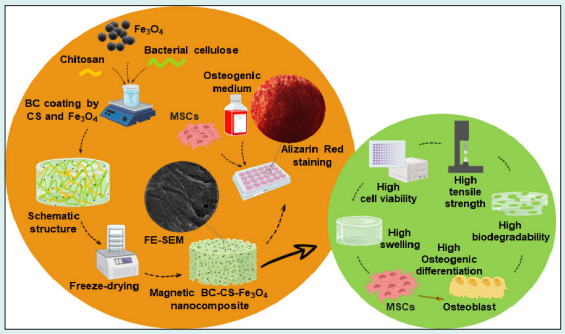

Introduction: Natural biopolymers are used for various purposes in healthcare, such as tissue engineering, drug delivery, and wound healing. Bacterial cellulose and chitosan were preferred in this study due to their non-cytotoxic, biodegradable, biocompatible, and non-inflammatory properties. The study reports the development of a magnetic bacterial cellulose-chitosan (BC-CS-Fe_3O_4) nanocomposite that can be used as a biocompatible scaffold for tissue engineering. Iron oxide nanoparticles were included in the composite to provide superparamagnetic properties that are useful in a variety of applications, including osteogenic differentiation, magnetic imaging, drug delivery, and thermal induction for cancer treatment.

Methods: The magnetic nanocomposite was prepared by immersing Fe_3O_4 in a mixture of bacterial cellulose-chitosan scaffold and then freeze-drying it. The resulting nanocomposite was characterized using FE-SEM and FTIR techniques. The swelling ratio and mechanical strength of the scaffolds were evaluated experimentally. The biodegradability of the scaffolds was assessed using PBS for 8 weeks at 37°C. The cytotoxicity and osteogenic differentiation of the nanocomposite were studied using human adipose-derived mesenchymal stem cells (ADSCs) and alizarin red staining. One-way ANOVA with Tukey's multiple comparisons test was used for statistical analysis.

Results: The FTIR spectra demonstrated the formation of bonds between functional groups of nanoparticles. FE-SEM images showed the integrity of the fibrillar network. The magnetic nanocomposite has the highest swelling ratio (2445% ± 23.34) and tensile strength (5.08 MPa). After 8 weeks, the biodegradation ratios of BC, BC-CS, and BC-CS-Fe_3O_4 scaffolds were 0.75% ± 0.35, 2.5% ± 0.1, and 9.5% ± 0.7, respectively. Magnetic nanocomposites have low toxicity ($P < 0.0001$) and higher osteogenic potential compared to other scaffolds.

Conclusion: Based on its high tensile strength, low water absorption, suitable degradability, low cytotoxicity, and high ability to induce an increase in calcium deposits by stem cells, the magnetic BC-CS-Fe_3O_4 nanocomposite scaffold can be a suitable candidate as a biomaterial for osteogenic differentiation.

Introduction

Polymer composites, nanocomposites, hydrogels, and bioceramics are used as scaffolds in tissue engineering.[1,2] The structure of scaffolds in tissue engineering, imitating the extracellular matrix, acts as a template to guide the growth of cells and ultimately tissue regeneration.[3] Repair in tissue engineering is accomplished through the appropriate use of cells, scaffolds, and cell growth-

*Corresponding authors: Neda Esfandiari, Email: ne_esfandiari@sbu.ac.ir; Soodabeh Davaran, Email: davaran@tbzmed.ac.ir

stimulating factors. Scaffolds provide the necessary support for the cells in terms of proliferation and differentiation into the desired tissue morphology and viability.[3,4] Biomaterials of natural and synthetic origin are utilized for a variety of functions, such as scaffolds for tissue engineering, drug delivery, wound healing, and many healthcare applications. Natural polymers are non-cytotoxicity, more biocompatible, less inflammatory and higher biodegradation rate than synthetic polymers. On the other hand, natural polymers have relatively weak mechanical properties, which can be improved by combining them with synthetic polymers.[5-7] To enhance the mechanical properties of various scaffolds in bone tissue engineering, synthetic polymers are often used and coated with natural-based polymers or extracellular matrix proteins.[8] Biopolymers are a suitable choice for various applications, including tissue engineering, implantation, wound healing, and drug delivery, due to their appropriate biochemical and biophysical properties in both in vivo and in vitro environments.[9] Biopolymers, when processed in the desired structure as a scaffold with special functions, can cause the differentiation of mesenchymal stem cells into target cells.[10] In fact, the type of biopolymer and scaffold design is very important for the successful differentiation of mesenchymal stem cells (MSCs) into target cells[10].

Bacterial cellulose (BC) is a natural biopolymer extracted from the bacterium *Gluconacetobacter xylinus*. BC possesses high porosity, excellent permeability, low density, a large surface area (10-50 nm in diameter and 100,000 nm in length),[11] suitable biocompatibility, high water retention capacity (up to 99%), enough heat stability, high crystallinity (70 to 80 percent), mechanical stability, and high purity.[12,13] Due to its fibrous structure and consequent pore size and shape,[14,15] optical transparency, non-toxicity, and the ability to mold into three-dimensional shapes and structures, researchers utilized BC fibers frequently in various scaffolds.[16,17] Characteristics including low biodegradability, high hydrophilicity, low compatibility with other hydrophobic polymers, and lack of antibacterial characteristics limit BC application as a single material.[18,19]

Chitosan (CS) is a cationic polymer, (due to the NH2-amino group) which is obtained through the deacetylation of chitin.[20] Interaction between the positive charges of CS and negatively charged molecules, such as proteoglycans, causes the formation of the extracellular matrix.[21-23] In addition, CS has several hydroxyl groups, which increase interaction with positively charged molecules.[24] Beyond NH2 groups, this improves mechanical and biological properties.[25] CS is the only cationic polysaccharide with a linear structure, suitable biocompatibility, biodegradability,[26] anti-inflammatory,[27,28] non-toxic,[29] anti-fungal,[30] antioxidant[31] properties, and self-healing activity.[32,33] Furthermore, it possesses anti-viral, anti-tumor,[34] anti-allergy,[35] anti-inflammatory,[36] wound healing, binding to red blood cells,[37] and hemocompatibility.[38]

For the first time, magnetic iron oxide (Fe_3O_4) nanoparticles were used in BC-CS nanocomposite to prepare a magnetic nanocomposite. Magnetic iron oxide (Fe_3O_4) nanoparticles in the range of 10-20 nm exhibit superparamagnetic properties and have various applications in biomedicine, including magnetic resonance imaging as contrast agents,[39,40] bone cell differentiation,[41] drug delivery,[42] tissue engineering,[43] treatment of fungal and bacterial diseases,[44,45] and regenerative medicine.[46] Therefore, in this study, BC hydrogel scaffolds were produced from *Gluconacetobacter xylinus* bacteria. Magnetic Fe_3O_4 nanoparticles were synthesized in the laboratory. By adding CS powder and magnetic Fe_3O_4 nanoparticles to the BC scaffold, a magnetic BC-CS-Fe_3O_4 nanocomposite was prepared using the immersion method. Since the BC-CS-Fe_3O_4 scaffold was not investigated in previous studies, we investigated the effect of the presence of Fe_3O_4 magnetic nanoparticles in the BC-CS scaffold on the physicochemical and morphological properties using Fourier transform infrared spectroscopy (FTIR) and field emission scanning electron microscopy (FE-SEM). Additionally, we evaluated the tensile strength and biodegradability ratio of the scaffolds. The cytotoxicity of the BC-CS-Fe_3O_4 magnetic scaffold was measured on human adipose-derived mesenchymal stem cells (ADSCs) compared to BC-CS and BC scaffolds. Furthermore, the amount of calcium deposits by ADSCs treated with the BC-CS-Fe_3O_4 magnetic scaffold, compared to BC-CS and BC scaffolds, was investigated using alizarin red staining. We expect that the BC-CS-Fe_3O_4 scaffold, as a novel magnetic nanocomposite with suitable physicochemical properties and high osteogenesis, is considered an ideal scaffold in tissue engineering.

Materials and Methods

Materials

Chitosan with a deacetylation degree of 70-85%, viscosity of 200-800 cp, and medium molecular weight was purchased from Sigma Aldrich, USA. Thiazolyl Blue Tetrazolium Bromide M5655 powder was also purchased from Sigma Aldrich, USA, and acetic acid was purchased from Merck, Germany. Dulbecco's modified Eagle medium (DMEM) with low glucose, osteogenesis differentiation medium (OsteoPlus), Alizarin Red S (1,2-Dihydroxyanthraquinone) staining solution, trypsin-EDTA enzyme, dimethyl sulfoxide (DMSO), and phosphate-buffered saline (PBS) solution (1 M, pH 7.4) from Bioidea (Idezist Notarkib), and fetal bovine serum (FBS) were purchased from Anacel, Iran. Iron(II) chloride and iron(III) chloride salts were purchased from Merck, Germany for the synthesis of magnetic (Fe_3O_4) nanoparticles. BC pellicles were also prepared in the laboratory under static conditions. The human adipose-derived mesenchymal stem cells (ADSCs) used in our study were obtained from Dr. Effat Alizadeh's cell culture

laboratory. The isolation, culture, and characterization of ADSCs were described in detail in their published articles.[47,48]

Production of bacterial cellulose (BC)

BC pellicles are produced by *Gluconacetobacter xylinus* bacteria colonies in Hestrin–Schramm (HS) medium.[49] The HS medium was used by mixing glucose (2% w/v), peptone (0.5% w/v), citric acid monohydrate (0.115% w/v), yeast extract (0.5% w/v), and di-sodium hydrogen phosphate dihydrate (0.27% w/v) using a proper method. The inoculum (10% v/v) was added to the HS culture medium with a pH of 5 and incubated for 14 days in the dark at 30°C. The produced pellicles were removed from the medium and immersed in a sodium hydroxide solution, and autoclaved to purify BC. To neutralize the pH, pellicles were washed and kept in distilled water (Fig. 1). Some of these pellicles were freeze-dried and characterized by FTIR and FE-SEM and examined by relevant tests.

Preparation of magnetic (Fe_3O_4) nanoparticle

To prepare magnetic (Fe_3O_4) nanoparticles, 20 ml of distilled water was added to 0.1 g of Fe(Cl)3 and 0.04 g of Fe(Cl)2 in a three-neck flask, which was placed on a magnetic stirrer at 50°C for 30 min. Then, 5 ml of 0.3 M NaOH was added to the solution, and gradually the color of the reaction changed from orange to black. After one hour, the synthesis of magnetic (Fe_3O_4) nanoparticles is completed. In order to remove the impurities, a relatively strong magnet is placed under the balloon. The supernatant solution containing water, NaOH, and unreacted substances is removed (Fig. 2).

Preparation of BC-CS nanocomposite scaffold

First, 0.5 g of CS powder was dissolved in 50 ml of 0.5% acetic acid. Then, 0.5 g of BC was added to the suspension, and the mixture was placed under a magnetic stirrer at 350 rpm overnight. The BC-CS nanocomposite scaffold was removed from the solution and utilized in the preparation of magnetic scaffolding.

Preparation of magnetic BC-CS-Fe_3O_4 nanocomposite scaffold

To prepare this scaffold, 0.5 g of CS was dissolved in 50 ml of 0.5% acetic acid. Then, 0.5 g of BC was added to the above solution, and 2 mg of magnetic (Fe_3O_4) nanoparticle powder was added to this mixture. The mixture was placed on the shaker overnight (Fig. 3). The magnetic BC-CS- Fe_3O_4 nanocomposite scaffold was removed from the solution and characterized by FTIR and FE-SEM after drying.

Characterization of produced materials

Fourier transforms infrared (FTIR)

The coating of CS and iron particles on cellulose and the evaluation of the bond formation between the functional groups of polymers and nanoparticles were investigated using FTIR from Bruker company, German.

Field emission scanning electron microscope (FE-SEM)

BC pellicle, BC-CS, and BC-CS-Fe_3O_4 nanocomposites were investigated to analyze the morphology and evaluate the CS and magnetic (Fe_3O_4) nanoparticle coating on BC fibrils using a field-emission scanning electron microscope (MIRA 3 FEG-SEM, Tescan company, Czech).

Mechanical test

The mechanical properties, such as tensile strength and Young's modulus, of the scaffolds studied in this research were determined using the ASTM D 638 tensile testing protocol of the Zwick Roell Zolo mechanical properties testing machine. Each sample was cut to a thickness of 1 mm and a size of 3 x 1.5 cm, and then stretched at a speed

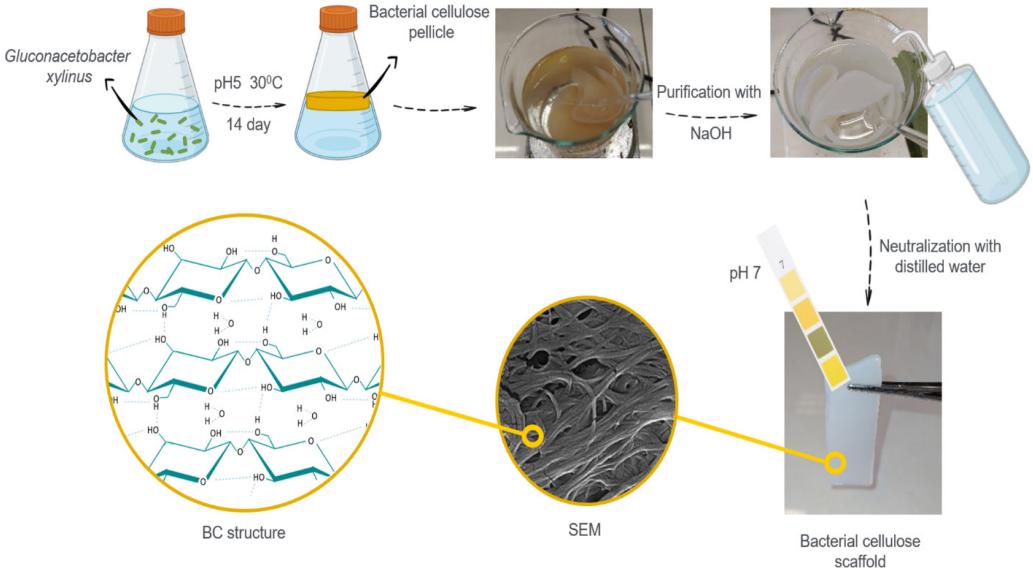

Fig. 1. The scheme of the synthesis of bacterial cellulose (BC) pellicle from *Gluconacetobacter xylinus* in static condition.

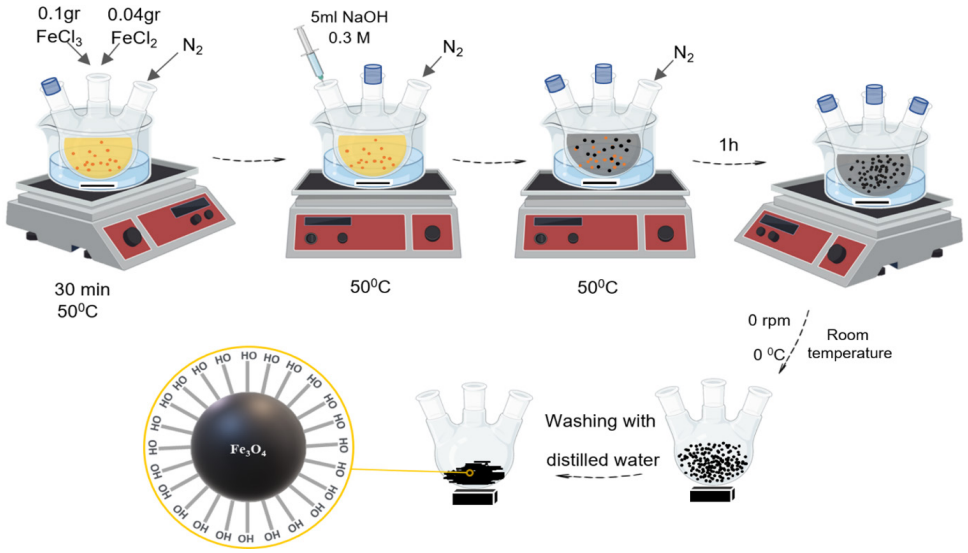

Fig. 2. The scheme of the synthesis of the magnetic (Fe_3O_4) nanoparticle using iron(III) chloride and iron(II) chloride.

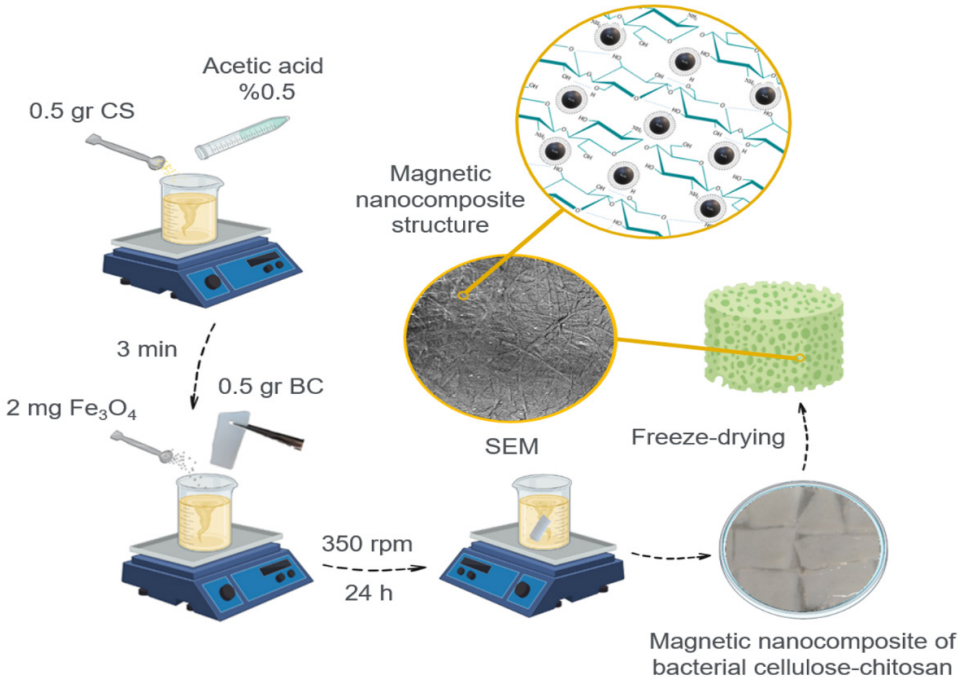

Fig. 3. The scheme of magnetic bacterial cellulose-chitosan-Fe_3O_4 nanocomposites scaffold.

of 5 mm/min with a force of 0.1 N to reach a constant stretching rate.

Swelling properties

To measure the swelling capacity of the scaffolds, 20 mg of dry BC, BC-CS, and BC-CS-Fe_3O_4 were cut (20 mm×20 mm) and were immersed in distilled water and phosphate-buffered saline (PBS) with pH 7.4, which was also selected as a swelling agent, separately. After removing at certain times, the surface water of the scaffolds was taken using cellulose filter paper, weighed, and finally, the amount of water absorption of each scaffold was calculated using Eq. 1. W_d represents the weight of the dry sample, and W_w represents the weight of the sample in the swollen state.

$$\%Swelling = \frac{Ww - Wd}{Wd} \times 100 \quad (1)$$

Biodegradability

In order to determine the ratio of biodegradability, 20 mg of each dry scaffold sample was immersed in 2 ml of PBS (1 M, pH 7.4) and incubated at 37°C for 8 weeks. For the investigation of the results in physiological conditions, PBS was used. At certain times, the scaffolds were removed from the PBS, the surface buffer was taken by cellulose filter paper, and the weight of the scaffold was measured.

Finally, the percentage of destruction of each scaffold was calculated using Eq. 2. W_0 is the initial dry weight of the sample, and W_t is the weight of the destroyed scaffold.

$$\%Degradation = \frac{Wt - W0}{W0} \times 100 \quad (2)$$

Cytotoxicity analysis

The MTT method was used to investigate the viability and proliferation of ADSCs as a result of the presence of BC and modified BC scaffolds. In addition, the cytotoxicity of CS powder and magnetic (Fe_3O_4) nanoparticles was evaluated as well. 200 µl of cell suspension (number of cells proportional to incubation time) were seeded separately in 96-well plates and incubated for 3, 5, and 7 days. After 24 hours of incubation, the cells attached to the surface of the plate, and the supernatant was discarded. Then, UV-sterilized BC, BC-CS, BC-CS-Fe_3O_4, CS, and Fe_3O_4 powder were placed inside the wells (3 replicates). The plate was wrapped in aluminum foil and incubated for 4 hours. After 4 hours, the medium (DMEM) of each well was transferred to the empty side wells, and 200 µl of dimethyl sulfoxide (DMSO) was added to each well and incubated for 20 minutes. Finally, the plate was transferred to the ELISA reader (Stat Fax 3200), and the absorption intensities were read at a wavelength of 540 nm.

Osteogenic differentiation of ADSCs

To investigate the effect of BC, CS powder, Fe_3O_4, and modified BC on the osteogenic differentiation of ADSCs, 2.5 x 105 cells were seeded in a 48-well plate. 200 µl of DMEM medium was added to each well and incubated at 37°C for 24 hours. Then, the medium of each well was discarded, and the scaffolds and powders that were previously sterilized with UV were placed in the wells in three replicates. 200 µl of osteogenic differentiation medium, based on the essential components of the ossification process, including dexamethasone, b-Glycerol phosphate, sodium pyruvate, and ascorbic acid, was added to each well. The medium was changed every three days for 21 days. Then, to study the results, Alizarin red staining was performed.

Characterization of osteogenic differentiation using Alizarin Red staining

Alizarin Red is used to identify bone cells containing calcium in MSC differentiation culture medium.[50] For staining, the culture medium was removed from all the wells and washed three times with PBS. To fix the cells, they were exposed to 4% formaldehyde for 15 minutes, then the formaldehyde was removed from the wells and washed three times with distilled water. Distilled water was completely removed, and 1 ml of Alizarin Red S dye was added to each well and incubated at 20-30°C with shaking. After incubation, the dyes of each well were discarded, and the wells were washed five times with distilled water. Imaging was then done using an inverted microscope. The obtained data were visually analyzed.

Statistical analysis

Statistical analysis was performed on the test results using one-way ANOVA (analysis of variance) with Tukey's multiple comparisons test. The statistical analyses were conducted using GraphPad Prism version 9.0.0. All experiments were performed in triplicate, and the results were presented as mean ± standard deviation. Statistically significant values were defined by * $P<0.05$, ** $P<0.01$, *** $P<0.001$, and **** $P<0.0001$.

Results and Discussion

Fourier transforms infrared (FTIR) analysis

FTIR spectroscopy was used to investigate the presence of polymers and magnetic (Fe_3O_4) nanoparticles and to ensure the formation of bonds between functional groups, the correct coating and loading of CS, and magnetic (Fe_3O_4) nanoparticles. The results are shown in Fig. 4. Due to the similarity of the molecular structure of BC and CS, their vibrations are very similar to each other. The O-H stretching vibration in the range of 3300 cm^{-1}-3500 cm^{-1} is shown in all samples. However, the relatively strong absorption of this vibration in CS powder is due to free OH groups. Intramolecular hydrogen bonding has been characterized by stretching vibration in the 3339 cm^{-1} wavenumber for cellulose. The absorption band in the range of 2894 cm^{-1}-2896 cm^{-1} represents the -CH bond, which indicates the amorphous nature of the scaffolds.[51] Absorption at 1106 cm^{-1} corresponds to the C-C stretching vibration in cellulose. The C-O-C stretching vibration in β-1-4 linkage is determined by absorption in the range of 1030 cm^{-1} to 1040 cm^{-1}. Absorption at 1315 cm^{-1} and 1427 cm^{-1}, and in the range of 1366 cm^{-1} to 1384 cm^{-1}, is related

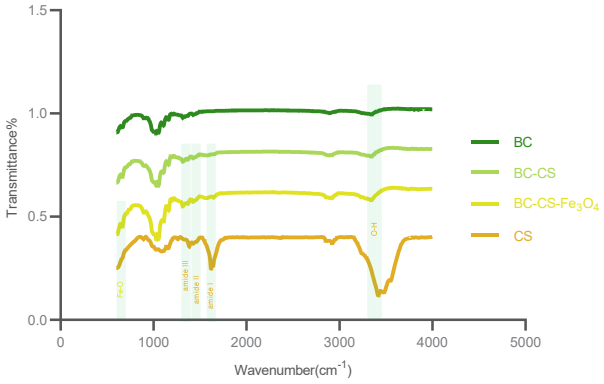

Fig. 4. Fourier transform infrared spectra were obtained for bacterial cellulose (BC), bacterial cellulose-chitosan (BC-CS), BC-CS-Fe_3O_4 scaffolds, CS and Fe_3O_4 powders. The structural similarity of BC and CS has caused similar vibrations. The strong absorption of the O-H stretching vibration at 3417 cm^{-1} in CS powder is due to free -OH groups. This vibration has been reduced in all scaffolds due to being involved in bonding with other functional groups. Amide I, amide II, and amide III are functional groups specific to chitosan with vibrations of 1618 cm^{-1}, 1550 cm^{-1}, and 1327 cm^{-1}, respectively, which indicate the presence of CS in BC fibers in nanocomposites. The Fe-O bond with an absorption of 664 cm^{-1} confirms the presence of Fe_3O_4 in the magnetic BC-CS-Fe_3O_4 nanocomposite.

to -OH bending vibration. The absorption at 1638 cm^{-1} corresponds to the N-H vibration in CS.

In the nanocomposites, vibrations related to amide I, amide II, and amide III were observed at 1613 cm^{-1}, 1550 cm^{-1}, and 1327 cm^{-1}, respectively, which are specific to CS molecules.[52] Due to the absence of amide vibrations in the bacterial cellulose (BC) scaffold, these vibrations in nanocomposites indicate the presence of CS in BC fibers. In the ternary composite, the C-O stretching vibration has absorption in the range of 1031 cm^{-1} to 1060 cm^{-1}. The wavelength in the range of 1427 cm^{-1} to 1576 cm^{-1} corresponds to the symmetric stretching of the -COO group. The Fe-O bond in the magnetic BC-CS-Fe_3O_4 nanocomposite was determined by an absorbance of 664 cm^{-1}, which indicates the correct loading of Fe_3O_4 nanoparticles in the BC-CS scaffold.

X-ray diffraction (XRD) and magnetization tests related to magnetic nanoparticles have been reported in our previous studies.[53,54]

Field emission scanning electron microscope (FE-SEM)

The FE-SEM image of BC, BC-CS, and BC-CS-Fe_3O_4 scaffolds with a resolution of 2µm and 500 nm is shown in Fig. 5. Fig. 5A clearly shows the fibrillar structure and well-organized networks of porous cellulose nanofibers. According to Fig. 5B, C, CS and Fe_3O_4 nanoparticles were successfully coated on cellulose fibers, and the network of BC nanofibers was completely preserved. The confirmation of the presence of CS in the magnetic BC-CS-Fe_3O_4 nanocomposite was determined by FTIR in Fig. 5 According to Fig. 5, the addition of CS and magnetic (Fe_3O_4) nanoparticles to the BC scaffold reduced the fibrillar structure of cellulose fibers in BC-CS (5B) and BC-CS-Fe_3O_4 (5C) nanocomposites. Other similar studies suggest that the addition of CS to the BC scaffold probably reduced the porosity in the BC-CS nanocomposite. This reduction is due to the placement of CS and magnetic (Fe_3O_4) nanoparticles in the pores of the cellulose scaffold and the interaction between the functional groups.[55] On the other hand, the presence of CS and magnetic (Fe_3O_4) nanoparticles increases the integrity of the scaffold, which is one of its important features. Similar results have been reported.[56,57]

Mechanical test

The mechanical characteristics of BC, BC-CS, and BC-CS-Fe_3O_4 scaffolds were evaluated using tensile tests and are presented in Table 1. The tensile strengths were found to be 1.19, 4.55, and 5.08 MPa for BC, BC-CS, and BC-CS-Fe_3O_4 scaffolds, respectively. The Young's modulus were 36.86, 23.76, and 3.89 MPa for BC, BC-CS, and BC-CS-Fe_3O_4 scaffolds, respectively. Based on the observations, modified BCs exhibited a decreased Young's modulus while the tensile strength increased. The Young's modulus represents the stiffness of the material, with a lower Young's modulus indicating higher strength against shocks and mechanical pressures. Similar results have been reported, showing an increase in tensile strength when modifying the BC scaffold.[52,58,59]

In a similar study, ZnO nanoparticles were used in a BC-CS nanocomposite. The results showed that the combination of CS in the BC fibrillar network increases the

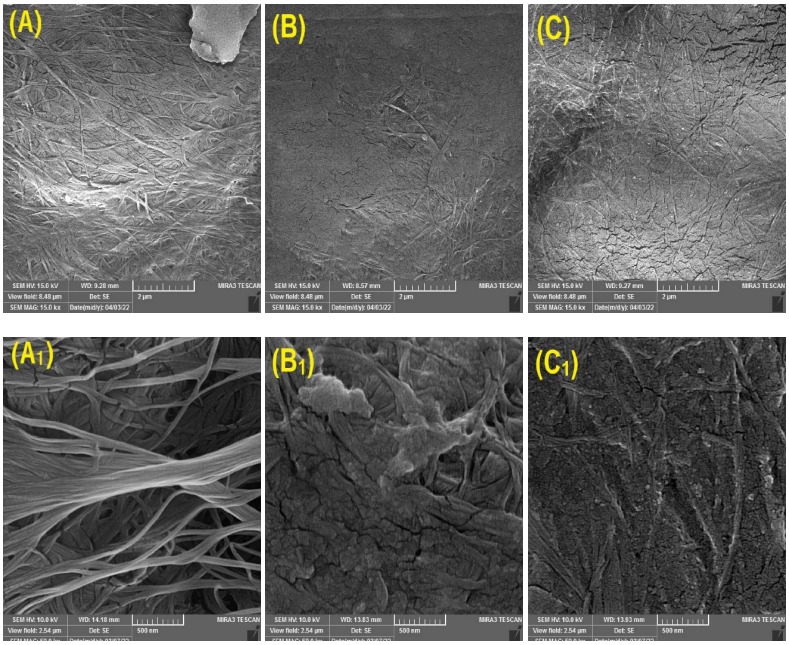

Fig. 5. FE-SEM morphology of **(A, A_1)** bacterial cellulose (BC); **(B, B_1)** bacterial cellulose-chitosan (BC-CS); **(C, C_1)** BC-CS-Fe_3O_4 scaffolds with 2 µm and 500nm resolution. **(A, A_1)** The BC scaffold had a completely fibrillar structure with high porosity. **(B, B_1)** The fibrillar structure in the BC-CS scaffold is reduced by the placement of CS among the cellulose strands, and the porosity is likely reduced as well. **(C, C_1)** The magnetic BC-CS-Fe_3O_4 nanocomposite has an interconnected network of BC, CS, and Fe_3O_4. Due to the presence of CS and Fe_3O_4 nanoparticles in the cellulose network of the BC scaffold, it has a more integrated structure than the BC and BC-CS scaffolds.

Table 1. Mechanical characterization of scaffolds

Sample	Young's modulus (MPa)	Tensile strength (MPa)
BC	36.86	1.19
BC-CS	23.76	4.55
BC-CS-Fe_3O_4	3.89	5.08

tensile strength of the scaffold. Additionally, the presence of nanoparticles in the BC-CS scaffold significantly increases the tensile strength.[60]

The obtained results are probably related to the formation of intermolecular hydrogen bonds between BC (-OH), CS (-OH and -NH2), and Fe_3O_4 (-O-), which limit the movement of the matrix while increasing its strength.[61] According to previous studies, the three-dimensional network of BC, which is the result of hydrogen bonding between the glucan chains of cellulose, increases the strength of the CS matrix by staggering in CS.[62]

Swelling properties

Water absorption is a sign of scaffold hydrophilicity and one of the practical features in tissue engineering. Hydrophilic polymers with physical or chemical cross-linking are ideal scaffolds in bone tissue engineering due to their ability to swell and form a three-dimensional structure for cell penetration and growth. Swelling of scaffolds improves mechanical stability and transport of gas and nutrients.[63] The swelling ratio of BC, BC-CS, and BC-CS-Fe_3O_4 scaffolds was reported as 2735%, 2321%, and 2445%, respectively.

The results in Fig. 6A show that BC has the highest

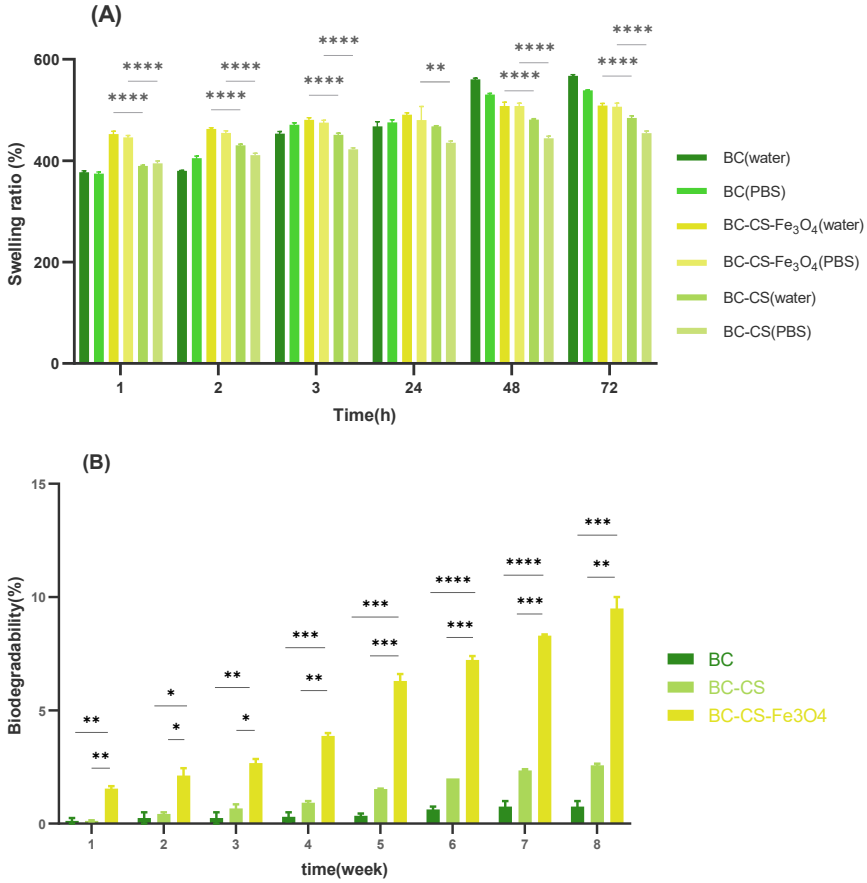

Fig. 6. The physicochemical characteristics for bacterial cellulose (BC), bacterial cellulose-chitosan (BC-CS), and magnetic BC-CS-Fe_3O_4 scaffolds: **(A)** swelling ratio, **(B)** biodegradability ratio. **(A)** The swelling ratio of scaffolds was measured by PBS (pH 7.4) for 72 hours. The swelling ratios of BC, BC-CS, and BC-CS-Fe_3O_4 scaffolds were 2735%, 2321%, and 2445%, respectively. The BC scaffold has the most OH functional groups and high hydrophilicity, resulting in the highest swelling ratio. It has the most hydrogen bonding with water molecules, which contributes to its high swelling ratio. The BC-CS nanocomposite has the lowest swelling ratio. This is due to the placement of CS in the cellulose network and the formation of hydrogen bonds between the amino groups of CS and the hydroxyls of BC, which reduces the number of hydroxyl groups and restricts the penetration of water into the BC-CS scaffold. On the other hand, the magnetic BC-CS-Fe_3O_4 nanocomposite has the highest swelling ratio among the modified BC scaffolds. This is because the formation of hydrogen bonds between the -O groups of Fe_3O_4 with water molecules has increased the number of hydroxyl groups. **(B)** Biodegradability ratio of scaffolds by PBS (pH 7.4) at 37°C for 8 weeks. In the 8th week, the biodegradability ratio of BC, BC-CS, and BC-CS-Fe_3O_4 scaffolds was 0.75% ± 0.35, 2.5% ± 0.1, and 9.5% ± 0.7, respectively. The presence of the amorphous structure of CS in the cellulose network of BC caused a disturbance in the crystalline structure of the BC scaffold, and the biodegradation ratio of the BC-CS scaffold has increased compared to the BC scaffold. The magnetic BC-CS-Fe_3O_4 nanocomposite had the highest degradation ratio. In addition to the amorphous structure of CS, due to the formation of Fe_3O_4 hydrogen bonds with CS and BC biopolymers, the crystalline structure of the nanocomposite was reduced. Groups were compared by one-way ANOVA (analysis of variance) with Tukey's multiple comparisons test using GraphPad Prism 9.0.0 software. Statistically significant values were defined by * $P < 0.05$, ** $P < 0.01$, *** $P < 0.001$, and **** $P < 0.0001$.

swelling ratio. This is likely due to the presence of OH groups in the structure of BC, as well as its high hydrophilic properties, resulting in a higher swelling ratio than the other scaffolds. The BC-CS scaffold has the lowest swelling ratio, possibly due to the penetration of CS among the cellulose fibers and the reduction of porosity in the BC scaffold. Additionally, the formation of hydrogen bonds between CS (–NH2) and BC (–OH), and the reduction of the number of -OH groups, may restrict water penetration into the BC-CS scaffold.[64] In other similar studies on BC and BC-CS scaffolds, the swelling results showed that the presence of CS in the BC cellulose network reduces porosity, thus reducing the swelling ratio of BC-CS scaffolds.[57,58] According to Fig. 6A, the magnetic BC-CS-Fe_3O_4 nanocomposite has the highest swelling ratio, after the BC scaffold. The magnetic BC-CS-Fe_3O_4 nanocomposite scaffold has a higher swelling ratio than the BC-CS nanocomposite scaffold, which probably increases the number of hydroxyl groups of the scaffold by forming hydrogen bonds between the -O groups of the magnetic (Fe_3O_4) nanoparticle and the water molecule. Therefore, it leads to more water absorption by the magnetic BC-CS-Fe_3O_4 nanocomposite scaffold. The magnetic nanocomposite is an ideal choice for use in tissue engineering due to its high water absorption and the specific characteristics of magnetic (Fe_3O_4) nanoparticles. Due to the high number of hydroxyl functional groups in water molecules, the swelling ratios of all samples in water were reported to be higher than those in PBS in each measurement.

Biodegradability

The biodegradability ratio of cellulose scaffolds was calculated using Eq. 2. In tissue engineering, polymers with different biodegradability ratios are used according to the type of damage and the tissue needed by the body. The results in Fig. 6B show the biodegradation ratio of the scaffolds over 8 weeks. In the 8th week, the biodegradability ratios of BC, BC-CS, and BC-CS-Fe_3O_4 scaffolds were 0.75% ± 0.35, 2.5% ± 0.1, and 9.5% ± 0.7, respectively. The BC scaffold has very little degradability compared to the BC-CS and BC-CS-Fe_3O_4 nanocomposites, and the magnetic BC-CS-Fe_3O_4 nanocomposite has the highest degradation ratio. The destruction of C-O-C bonds is the main reason for the degradation of BC fibers.[65] The difference in degradation ratio can probably be related to the structure of the polymers in the scaffold. In the crystal structure, the atoms are regularly placed next to each other, and the identical intermolecular and atomic forces keep the components of a material together. While the atoms of the amorphous structure are irregularly placed next to each other, the difference in the placement of atoms causes a difference in material properties such as the melting point, degradability ratio, and other properties related to the structure of the material.[66,67]

In studies similar to this research, the degradability ratio of the BC scaffold is lower than that of the BC-CS nanocomposite scaffold because the hydrogen bonds between cellulose fibers create a firm cellulose network. The penetration of CS into the cellulose network disrupts the main hydrogen bonds and, by causing irregularities, reduces the crystal index of BC. As a result, the ratio of biodegradability in the BC-CS nanocomposite scaffold increases.[19,68]

In another study, the biodegradability ratio of BC, BC-CS, and BC-CS-G (gelatin) scaffolds was investigated. Due to the low rate of degradation of the crystalline structure of BC compared to the amorphous and semi-crystalline structure of CS and G, the percentage of biodegradability of BC-CS is higher than the BC scaffold.[52] Therefore, in this research, the presence of the amorphous structure of CS among the crystal structure of BC has decreased the crystallinity index of BC in the BC-CS scaffold, and the biodegradation ratio has increased compared to the pure cellulose scaffold. In the magnetic BC-CS-Fe_3O_4 nanocomposite scaffold, due to the formation of hydrogen bonds between CS simultaneously with BC and Fe_3O_4 nanoparticles, the crystal structure is disturbed. Since the degradation ratio of the amorphous structure is higher than the crystal structure, the biodegradation ratio of the magnetic BC-CS-Fe_3O_4 nanocomposite scaffold compared to BC and BC-CS has increased.

Cytotoxicity test

The results of cytotoxicity assays (MTT) are shown in Fig. 7. The UV absorption intensity of the ADSCs treated with BC, BC-CS, and magnetic BC-CS-Fe_3O_4 nanocomposite scaffolds was higher than that of the untreated ADSCs (control), indicating an increase in the percentage of cell viability. The percentage of cell viability treated with the magnetic BC-CS-Fe_3O_4 nanocomposite scaffold on days 3, 5, and 7 was reported to be 115%, 125%, and 129%, respectively. For the BC-CS nanocomposite, the percentage of cell viability was 111%, 119%, and 118% on days 3, 5, and 7, respectively. According to Fig. 7, the magnetic BC-CS-Fe_3O_4 nanocomposite scaffold showed a significant difference in the percentage of cell viability compared to all groups. This result is probably a consequence of the increase in the -OH of the BC-CS-Fe_3O_4 scaffold compared to the BC-CS and BC-CS-Fe_3O_4 scaffolds. In addition, the antimicrobial properties of Fe_3O_4 may have led to an increase in cell proliferation.[69] Also, cell adhesion enhancement has been reported in some studies in the presence of CS[70]; these properties together increase the viability, growth, and proliferation of the cells. In other studies, the viability of hASCs treated with pure BC and BC/magnetic nanocomposites with 1%, 2%, and 5% of Fe_3O_4 for 24 hours and 5 days was investigated. A significant difference was observed in the viability of cells exposed to pure BC and BC/Fe_3O_4. The results showed that

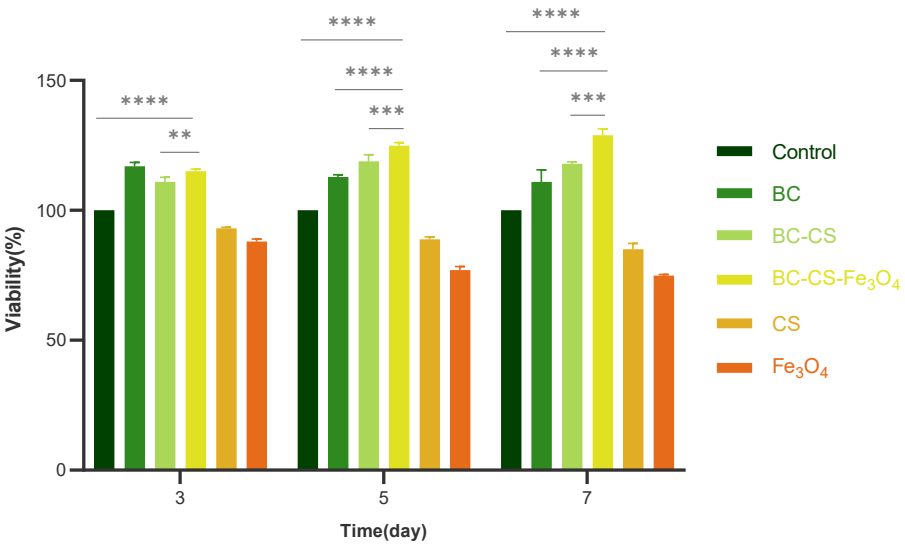

Fig. 7. MTT assay was performed on ADSCs cultivated on BC, BC-CS, and BC-CS-Fe_3O_4 scaffolds for 3, 5, and 7 days. The percentage of cell viability treated with the magnetic BC-CS-Fe_3O_4 nanocomposite showed a significant difference compared to the other groups. The percentage of cell viability treated with the magnetic BC-CS-Fe_3O_4 nanocomposite scaffold on days 3, 5, and 7 was reported to be 115%, 125%, and 129%, respectively. Due to the increase in hydroxyl group and the special properties of BC and CS biopolymers, as well as the antibacterial property of Fe_3O_4, the percentage of cell viability treated with the magnetic BC-CS-Fe_3O_4 nanocomposite increased. Groups were compared by one-way ANOVA (analysis of variance) with Tukey's multiple comparisons test using GraphPad Prism 9.0.0 software. Statistically significant values were defined by * $P < 0.05$, ** $P < 0.01$, *** $P < 0.001$, and **** $P < 0.0001$.

with the increase in magnetic percentage, the cell viability also increases.[71] Magnetic BC-CS-Fe_3O_4 nanocomposite scaffold possesses the highest optical absorption and the lowest cytotoxicity compared to other samples, making it a suitable scaffold for the growth and proliferation of cells in bone tissue engineering.

Osteogenic differentiation of ADSCs

In order to investigate the scaffolds' role in increasing the differentiation of mesenchymal stem cells into osteogenic cells, the ADSCs were treated with the developed scaffolds and compared with the untreated ADSCs (control). The images of cells stained with alizarin red and captured using an inverted microscope are depicted in Fig. 8. The deposition of late osteogenesis markers, such as calcium phosphate, can be observed around the cells of all samples in Fig. 8. Calcium deposits serve as evidence for osteogenesis in various studies.[72-74]

Both BC and CS enhance the osteogenic differentiation of bone.[75,76] In other research, the outcomes of the osteogenic differentiation of ADSCs treated with BC and CS, as well as CS/carboxymethyl cellulose/nanohydroxyapatite scaffolds, following 14 days of alizarin red staining, indicated that the osteogenic capacity of each of the BC and CS scaffolds was inferior to that of the composite form.[77-79]

Microscopic images (Fig. 8 C_1, C_2, C_3) show increased calcium deposits in the presence of magnetic BC-CS-Fe_3O_4 nanocomposite scaffolds compared to other scaffolds. According to previous studies, Fe_3O_4 leads to enhanced Runx2 gene expression.[80,81] Runx2 is the main gene controlling osteoblast differentiation and is required for the expression of several osteogenic genes, including collagen I, osteopontin, alkaline phosphatase, and osteocalcin.[82,83]

Conclusion

Magnetic BC-CS-Fe_3O_4 nanocomposite scaffolds were successfully prepared for the first time in this research. This nanocomposite is made of natural, non-toxic polymers BC and CS. The BC-CS scaffold was prepared by adding magnetic (Fe_3O_4) nanoparticles for the first time. The FTIR vibrations confirmed the bonding among CS functional groups, magnetic nanoparticles (Fe_3O_4), and cellulose fibers. The FE-SEM results demonstrated the integrity of the fibrillar surface of the magnetic scaffold. The tensile strength of the magnetic BC-CS-Fe_3O_4 nanocomposite scaffold increased, probably due to the increased bonding between the functional groups of BC and CS and the magnetic (Fe_3O_4) nanoparticles.

The magnetic BC-CS-Fe_3O_4 scaffold showed higher water absorption than the BC-CS scaffold Magnetic nanocomposites had a higher biodegradability ratio than BC and BC-CS scaffolds. The BC-CS-Fe_3O_4 magnetic nanocomposite had the least cytotoxicity on ADSCs. The magnetic BC-CS-Fe_3O_4 nanocomposite scaffold resulted in significantly higher calcium deposit formation during osteogenic differentiation of ADSCs compared to other scaffolds. The magnetic BC-CS-Fe_3O_4 nanocomposite showed high water absorption and mechanical strength, high osteogenic differentiation, low cytotoxicity and high biodegradability compared to BC-CS and BC scaffolds, enabling in vivo mimicry.

The properties of the BC-CS-Fe3O4 magnetic

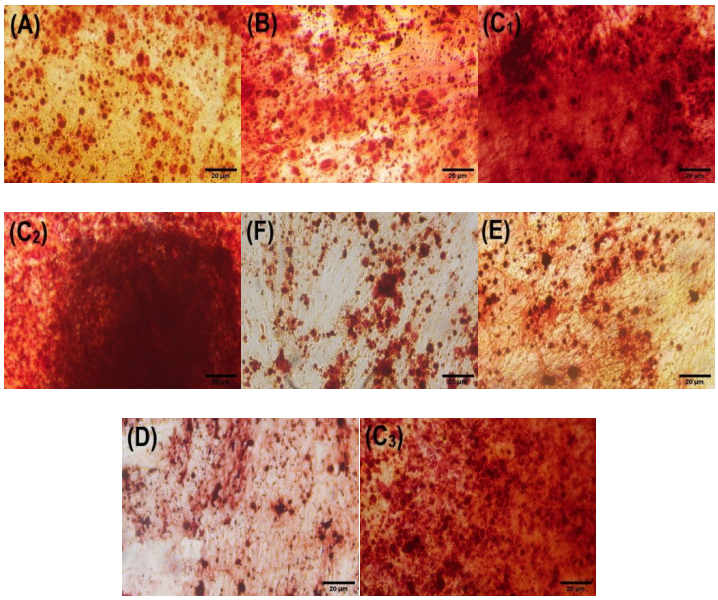

Fig. 8. Alizarin Red staining was performed on day 21 to investigate the calcium deposits resulting from the osteogenic differentiation of ADMCs cells treated with (A) BC; (B) BC-CS; (C1, C2, C3) BC-CS-Fe_3O_4 (scaffold); (D) CS; (E) Fe_3O_4 (powder); (F) control. The obtained data were visually analyzed with an inverted microscope. According to the images, ADSCs cells treated with the magnetic BC-CS-Fe_3O_4 nanocomposite had the highest dye intensity of calcium deposits. The ADSCs cells treated with CS and Fe_3O_4 nanoparticles exhibited the lowest dye intensity of calcium deposits.

nanocomposite are expected to make it a promising candidate for biomedical applications, such as osteogenic differentiation, wound healing, and magnetically guided drug delivery.

Acknowledgment

We would like to thank the Drug Applied Research center (DARC), Tabriz University of Medical Sciences (Tabriz, Iran), and Iran National Science Foundation (INSF, Granted research Chair Awards) for their support and help.

Authors' contribution:

Conceptualization: Nahid Rezazadeh.
Data curation: Nahid Rezazadeh, Effat Alizadeh, Soodabeh Davaran, Neda Esfandiari.
Formal analysis: Nahid Rezazadeh.
Funding acquisition: Nahid Rezazadeh, Effat Alizadeh, Soodabeh Davaran, Neda Esfandiari.
Investigation: Nahid Rezazadeh.
Methodology: Soodabeh Davaran, Neda Esfandiari.
Project administration: Soodabeh Davaran, Neda Esfandiari.
Resources: Nahid Rezazadeh.
Supervision: Soodabeh Davaran, Neda Esfandiari.
Validation: Nahid Rezazadeh, Effat Alizadeh, Somaieh Soltani, Soodabeh Davaran, Neda Esfandiari.
Visualization: Nahid Rezazadeh, Soodabeh Davaran.
Writing–original draft: Nahid Rezazadeh.
Writing–review & editing: Somaieh Soltani, Soodabeh Davaran, Neda Esfandiari.

Research Highlights

What is the current knowledge?

√ A magnetic bacterial cellulose-chitosan-Fe_3O_4 nanocomposite scaffold based on natural and non-toxic polymers was prepared as a biocompatible and biodegradable scaffold in bone tissue engineering

What is new here?

√ The addition of magnetic (Fe3O4) nanoparticles to the bacterial cellulose-chitosan nanocomposite scaffold was done for the first time in this study.

√ The superparamagnetic properties of Fe3O4 significantly increase water absorption, mechanical strength, cell viability, and biodegradability, which can mimic in vivo conditions.

√ The high osteogenic potential was reported for mesenchymal stem cells treated with magnetic nanocomposites.

√ The magnetic properties of this bacterial cellulose-chitosan nanocomposite make it an appropriate candidate for biomedical applications such as osteogenic differentiation.

Competing interests

The authors declare that they have no potential conflicts of interest.

Ethical Statement

Not applicable for this paper.

Funding

None.

References

1. Ullah S, Chen X. Fabrication, applications and challenges of natural biomaterials in tissue engineering. *Appl Mater Today* **2020**; 20: 100656. https://doi.org/10.1016/j.apmt.2020.100656
2. Xue X, Hu Y, Deng Y, Su J. Recent advances in design of functional biocompatible hydrogels for bone tissue engineering. *Adv Funct Mater* **2021**; 31: 2009432. https://doi.org/10.1002/adfm.202009432
3. O'brien FJ. Biomaterials & scaffolds for tissue engineering. *Materials Today* **2011**; 14: 88-95. https://doi.org/10.1016/S1369-7021(11)70058-X
4. Choi S-W, Zhang Y, Xia Y. Three-dimensional scaffolds for tissue engineering: the importance of uniformity in pore size and structure. *Langmuir* **2010**; 26: 19001-6. https://doi.org/10.1021/la104206h
5. MM S. Biomaterials for bone materials tissue engineering. *Mater Today* **2008**; 11: 18-25. https://doi.org/10.1016/S1369-

7021(08)70086-5
6. Li X, Wang L, Fan Y, Feng Q, Cui FZ, Watari F. Nanostructured scaffolds for bone tissue engineering. *J Biomed Mater Res A* **2013**; 101: 2424-35. https://doi.org/10.1002/jbm.a.34539
7. Haugen HJ, Lyngstadaas SP, Rossi F, Perale G. Bone grafts: which is the ideal biomaterial? *J Clin Periodontol* **2019**; 46: 92-102. https://doi.org/10.1111/jcpe.13058
8. Li X, Xie J, Yuan X, Xia Y. Coating electrospun poly (ε-caprolactone) fibers with gelatin and calcium phosphate and their use as biomimetic scaffolds for bone tissue engineering. *Langmuir* **2008**; 24: 14145-50. https://doi.org/10.1021/la802984a
9. Pina S, Reis RL, Oliveira JM. Natural polymeric biomaterials for tissue engineering. *Tissue Engineering Using Ceramics and Polymers*: Elsevier; **2022**. p. 75-110. https://doi.org/10.1016/B978-0-12-820508-2.00001-5
10. Noh YK, Dos Santos Da Costa A, Park YS, Du P, Kim IH, Park K. Fabrication of bacterial cellulose-collagen composite scaffolds and their osteogenic effect on human mesenchymal stem cells. *Carbohydr Polym* **2019**; 219: 210-8. https://doi.org/10.1016/j.carbpol.2019.05.039
11. Choi SM, Shin EJ. The nanofication and functionalization of bacterial cellulose and its applications. *Nanomaterials* **2020**; 10: 406. https://doi.org/10.3390/nano10030406
12. Ul-Islam M, Subhan F, Islam SU, Khan S, Shah N, Manan S, *et al.* Development of three-dimensional bacterial cellulose/chitosan scaffolds: Analysis of cell-scaffold interaction for potential application in the diagnosis of ovarian cancer. *Int J Biol Macromol* **2019**; 137: 1050-9. https://doi.org/10.1016/j.ijbiomac.2019.07.050
13. Di Z, Shi Z, Ullah MW, Li S, Yang G. A transparent wound dressing based on bacterial cellulose whisker and poly (2-hydroxyethyl methacrylate). *Int J Biol Macromol* **2017**; 105: 638-44. https://doi.org/10.1016/j.ijbiomac.2017.07.075
14. Shah N, Ul-Islam M, Khattak WA, Park JK. Overview of bacterial cellulose composites: a multipurpose advanced material. *Carbohydr Polym* **2013**; 98: 1585-98. https://doi.org/10.1016/j.carbpol.2013.08.018
15. Lee K-Y. *Nanocellulose and sustainability: production, properties, applications, and case studies*: CRC Press; **2018**.
16. Picheth GF, Pirich CL, Sierakowski MR, Woehl MA, Sakakibara CN, de Souza CF, *et al.* Bacterial cellulose in biomedical applications: A review. *Int J Biol Macromol* **2017**; 104: 97-106. https://doi.org/10.1016/j.ijbiomac.2017.05.171
17. Lin N, Dufresne A. Nanocellulose in biomedicine: Current status and future prospect. *Eur Polym J* **2014**; 59: 302-25. https://doi.org/10.1016/j.eurpolymj.2014.07.025
18. Li Z, Ma J, Li R, Yin X, Dong W, Pan C. Fabrication of a blood compatible composite membrane from chitosan nanoparticles, ethyl cellulose and bacterial cellulose sulfate. *RSC Adv* **2018**; 8: 31322-30. https://doi.org/10.1039/C8RA05536J
19. Yin N, Du R, Zhao F, Han Y, Zhou Z. Characterization of antibacterial bacterial cellulose composite membranes modified with chitosan or chitooligosaccharide. *Carbohydr Polym* **2020**; 229: 115520. https://doi.org/10.1016/j.carbpol.2019.115520
20. Naveed M, Phil L, Sohail M, Hasnat M, Baig MMFA, Ihsan AU, *et al.* Chitosan oligosaccharide (COS): An overview. *Int J Biol Macromol* **2019**; 129: 827-43. https://doi.org/10.1016/j.ijbiomac.2019.01.192
21. Kean T, Thanou M. Chitin and chitosan: sources, production and medical applications. In: Williams P, ed. *Renewable resources for functional polymers and biomaterials.* Royal Society of Chemistry: **2011**. p. 292-318. https://doi.org/10.1039/9781849733519-00292.
22. Younes I, Rinaudo M. Chitin and chitosan preparation from marine sources. Structure, properties and applications. *Mar Drugs* **2015**; 13: 1133-74. https://doi.org/10.3390/md13031133
23. Sivashankari P, Prabaharan M. Prospects of chitosan-based scaffolds for growth factor release in tissue engineering. *Int J Biol Macromol* **2016**; 93: 1382-9. https://doi.org/10.1016/j.ijbiomac.2016.02.043
24. Rahmani Del Bakhshayesh A, Annabi N, Khalilov R, Akbarzadeh A, Samiei M, Alizadeh E, *et al.* Recent advances on biomedical applications of scaffolds in wound healing and dermal tissue engineering. *Artif Cells Nanomed Biotechnol* **2018**; 46: 691-705. https://doi.org/10.1080/21691401.2017.1349778
25. Ruiz GA, Corrales HF. Chitosan, chitosan derivatives and their biomedical applications. *Biological activities and application of marine polysaccharides*. IntechOpen; **2017**. p. 87. https://doi.org/10.5772/66527.
26. Phil L, Naveed M, Mohammad IS, Bo L, Bin D. Chitooligosaccharide: An evaluation of physicochemical and biological properties with the proposition for determination of thermal degradation products. *Biomed Pharmacother* **2018**; 102: 438-51. https://doi.org/10.1016/j.biopha.2018.03.108
27. Chung MJ, Park JK, Park YI. Anti-inflammatory effects of low-molecular weight chitosan oligosaccharides in IgE–antigen complex-stimulated RBL-2H3 cells and asthma model mice. *Int Immunopharmacol* **2012**; 12: 453-9. https://doi.org/10.1016/j.intimp.2011.12.027
28. Yang E-J, Kim J-G, Kim J-Y, Kim SC, Lee NH, Hyun C-G. Anti-inflammatory effect of chitosan oligosaccharides in RAW 264.7 cells. *Cent Eur J Biol* **2010**; 5: 95-102. https://doi.org/10.2478/s11535-009-0066-5
29. Wahid F, Hu X-H, Chu L-Q, Jia S-R, Xie Y-Y, Zhong C. Development of bacterial cellulose/chitosan based semi-interpenetrating hydrogels with improved mechanical and antibacterial properties. *Int J Biol Macromol* **2019**; 122: 380-7. https://doi.org/10.1016/j.ijbiomac.2018.10.105
30. Basseri H, Bakhtiyari R, Hashemi SJ, Baniardelani M, Shahraki H, Hosainpour L. Antibacterial/antifungal activity of extracted chitosan from American cockroach (Dictyoptera: Blattidae) and German cockroach (Blattodea: Blattellidae). *J Med Entomol* **2019**; 56: 1208-14. https://doi.org/10.1093/jme/tjz082
31. Chang S-H, Wu C-H, Tsai G-J. Effects of chitosan molecular weight on its antioxidant and antimutagenic properties. *Carbohydr Polym* **2018**; 181: 1026-32. https://doi.org/10.1016/j.carbpol.2017.11.047
32. Wang S, Urban MW. Self-healing polymers. *Nat Rev Mater* **2020**; 5: 562-83. https://doi.org/10.1038/s41578-020-0202-4
33. Cheng K-C, Huang C-F, Wei Y, Hsu S-h. Novel chitosan–cellulose nanofiber self-healing hydrogels to correlate self-healing properties of hydrogels with neural regeneration effects. *NPG Asia Mater* **2019**; 11: 1-17. https://doi.org/10.1038/s41427-019-0124-z
34. Abd Elgadir M, Uddin MS, Ferdosh S, Adam A, Chowdhury AJK, Sarker MZI. Impact of chitosan composites and chitosan nanoparticle composites on various drug delivery systems: A review. *J **Food Drug** Anal* **2015**; 23: 619-29. https://doi.org/10.1016/j.jfda.2014.10.008
35. Xie C, Wu X, Long C, Wang Q, Fan Z, Li S, *et al.* Chitosan oligosaccharide affects antioxidant defense capacity and placental amino acids transport of sows. *BMC Vet Res* **2016**; 12: 1-8. https://doi.org/10.1186/s12917-016-0872-8
36. Mohyuddin SG, Qamar A, Hu C-y, Chen S-W, Wen J-y, Liu X-x, *et al.* Effect of chitosan on blood profile, inflammatory cytokines by activating TLR4/NF-κB signaling pathway in intestine of heat stressed mice. *Sci Rep* **2021**; 11: 1-13. https://doi.org/10.1038/s41598-021-98931-8
37. Azuma K, Izumi R, Osaki T, Ifuku S, Morimoto M, Saimoto H, *et al.* Chitin, chitosan, and its derivatives for wound healing: old and new materials. *J Funct Biomater* **2015**; 6: 104-42. https://doi.org/10.3390/jfb6010104
38. Balan V, Verestiuc L. Strategies to improve chitosan hemocompatibility: A review. *Eur Polym J* **2014**; 53: 171-88. https://doi.org/10.1016/j.eurpolymj.2014.01.033
39. Olsvik O, Popovic T, Skjerve E, Cudjoe KS, Hornes E, Ugelstad J, *et al.* Magnetic separation techniques in diagnostic microbiology. *Clin Microbiol Rev* **1994**; 7: 43-54. https://doi.org/10.1128/cmr.7.1.43
40. Yeh TC, Zhang W, Ildstad ST, Ho C. Intracellular labeling of T-cells with superparamagnetic contrast agents. *Magn Reson Med* **1993**; 30: 617-25. https://doi.org/10.1002/mrm.1910300513
41. Arias LS, Pessan JP, Vieira APM, Lima TMTd, Delbem ACB,

Monteiro DR. Iron oxide nanoparticles for biomedical applications: A perspective on synthesis, drugs, antimicrobial activity, and toxicity. *Antibiotics* **2018**; 7: 46. https://doi.org/10.3390/antibiotics7020046

42. Mu Q, Kievit FM, Kant RJ, Lin G, Jeon M, Zhang M. Anti-HER2/neu peptide-conjugated iron oxide nanoparticles for targeted delivery of paclitaxel to breast cancer cells. ***Nanoscale*** **2015**; 7: 18010-4. https://doi.org/10.1039/C5NR04867B
43. Pinaud F, King D, Moore H-P, Weiss S. Bioactivation and cell targeting of semiconductor CdSe/ZnS nanocrystals with phytochelatin-related peptides. *J Am Chem Soc* **2004**; 126: 6115-23. https://doi.org/10.1021/ja031691c
44. Ivashchenko O, Jurga-Stopa J, Coy E, Peplinska B, Pietralik Z, Jurga S. Fourier transform infrared and Raman spectroscopy studies on magnetite/Ag/antibiotic nanocomposites. *Appl Surf Sci* **2016**; 364: 400-9. https://doi.org/10.1016/j.apsusc.2015.12.149
45. Johnson GA, Benveniste H, Black R, Hedlund L, Maronpot R, Smith B. Histology by magnetic resonance microscopy. *Magn Reson Q* **1993**; 9: 1-30.
46. Dumestre F, Chaudret B, Amiens C, Fromen MC, Casanove MJ, Renaud P, *et al.* Shape control of thermodynamically stable cobalt nanorods through organometallic chemistry. *Angewandte Chemie International Edition* **2002**; 41: 4286-9. https://doi.org/10.1002/1521-3773(20021115)41:22%3C4286::AID-ANIE4286%3E3.0.CO;2-M
47. Alizadeh E, Zarghami N, Eslaminejad MB, Akbarzadeh A, Barzegar A, Mohammadi SA. The effect of dimethyl sulfoxide on hepatic differentiation of mesenchymal stem cells. *Artif* ***Cells*** *Nanomed Biotechnol* **2016**; 44: 157-64. https://doi.org/10.3109/21691401.2014.928778
48. Hoseinzadeh S, Atashi A, Soleimani M, Alizadeh E, Zarghami N. MiR-221-inhibited adipose tissue-derived mesenchymal stem cells bioengineered in a nano-hydroxy apatite scaffold. *In Vitro Cell Dev Biol Anim* **2016**; 52: 479-87. https://doi.org/10.1007/s11626-015-9992-x
49. Khan S, Ul-Islam M, Khattak WA, Ullah MW, Park JK. Bacterial cellulose-titanium dioxide nanocomposites: nanostructural characteristics, antibacterial mechanism, and biocompatibility. *Cellulose* **2015**; 22: 565-79. https://doi.org/10.1007/s10570-014-0528-4
50. Elkhenany H, Amelse L, Caldwell M, Abdelwahed R, Dhar M. Impact of the source and serial passaging of goat mesenchymal stem cells on osteogenic differentiation potential: implications for bone tissue engineering. *J Anim Sci Biotechnol* **2016**; 7: 1-13. https://doi.org/10.1186/s40104-016-0074-z
51. Goh W, Rosma A, Kaur B, Fazilah A, Karim A, Bhat R. Microstructure and physical properties of microbial cellulose produced during fermentation of black tea broth (Kombucha). II. *Int Food Res J* **2012**; 19: 153.
52. Sharma C, Bhardwaj NK, Pathak P. Ternary nano-biocomposite films using synergistic combination of bacterial cellulose with chitosan and gelatin for tissue engineering applications. *J Biomater Sci Polym Ed* **2021**; 32: 166-88. https://doi.org/10.1080/09205063.2020.1822122
53. Sadr SH, Davaran S, Alizadeh E, Salehi R, Ramazani A. PLA-based magnetic nanoparticles armed with thermo/pH responsive polymers for combination cancer chemotherapy. *J Drug Deliv Sci Technol* **2018**; 45: 240-54. https://doi.org/10.1016/j.jddst.2018.03.019
54. Nosrati H, Salehiabar M, Fridoni M, Abdollahifar M-A, Kheiri Manjili H, Davaran S, *et al.* New insight about biocompatibility and biodegradability of iron oxide magnetic nanoparticles: stereological and in vivo MRI monitor. *Sci Rep* **2019**; 9: 7173. https://doi.org/10.1038/s41598-019-43650-4
55. Cacicedo ML, Pacheco G, Islan GA, Alvarez VA, Barud HS, Castro GR. Chitosan-bacterial cellulose patch of ciprofloxacin for wound dressing: Preparation and characterization studies. *Int J Biol Macromol* **2020**; 147: 1136-45. https://doi.org/10.1016/j.ijbiomac.2019.10.082
56. Li G, Nandgaonkar AG, Habibi Y, Krause WE, Wei Q, Lucia LA. An environmentally benign approach to achieving vectorial alignment and high microporosity in bacterial cellulose/chitosan scaffolds. ***RSC*** *Adv* **2017**; 7: 13678-88. https://doi.org/10.1039/C6RA26049G
57. Lin W-C, Lien C-C, Yeh H-J, Yu C-M, Hsu S-h. Bacterial cellulose and bacterial cellulose–chitosan membranes for wound dressing applications. *Carbohydr Polym* **2013**; 94: 603-11. https://doi.org/10.1016/j.carbpol.2013.01.076
58. Zhao H, Zhang L, Zheng S, Chai S, Wei J, Zhong L, *et al.* Bacteriostatic activity and cytotoxicity of bacterial cellulose-chitosan film loaded with in-situ synthesized silver nanoparticles. *Carbohydr Polym* **2022**; 281: 119017. https://doi.org/10.1016/j.carbpol.2021.119017
59. Ul-Islam M, Khan T, Park JK. Water holding and release properties of bacterial cellulose obtained by in situ and ex situ modification. *Carbohydr Polym* **2012**; 88: 596-603. https://doi.org/10.1016/j.carbpol.2012.01.006
60. Kai J, Xuesong Z. Preparation, characterization, and cytotoxicity evaluation of zinc oxide–bacterial cellulose–chitosan hydrogels for antibacterial dressing. *Macromol Chem Phys* **2020**; 221: 2000257. https://doi.org/10.1002/macp.202000257
61. Urbina L, Guaresti O, Requies J, Gabilondo N, Eceiza A, Corcuera MA, *et al.* Design of reusable novel membranes based on bacterial cellulose and chitosan for the filtration of copper in wastewaters. *Carbohydr Polym* **2018**; 193: 362-72. https://doi.org/10.1016/j.carbpol.2018.04.007
62. Liang J, Wang R, Chen R. The impact of cross-linking mode on the physical and antimicrobial properties of a chitosan/bacterial cellulose composite. ***Polymers*** *(Basel)* **2019**; 11: 491. https://doi.org/10.3390/polym11030491
63. Sreekumaran S, Radhakrishnan A, Rauf AA, Kurup GM. Nanohydroxyapatite incorporated photocrosslinked gelatin methacryloyl/poly(ethylene glycol)diacrylate hydrogel for bone tissue engineering. *Prog Biomater* **2021**; 10: 43-51. https://doi.org/10.1007/s40204-021-00150-x
64. Wichai S, Chuysinuan P, Chaiarwut S, Ekabutr P, Supaphol P. Development of bacterial cellulose/alginate/chitosan composites incorporating copper (II) sulfate as an antibacterial wound dressing. *J Drug Deliv Sci Technol* **2019**; 51: 662-71. https://doi.org/10.1016/j.jddst.2019.03.043
65. Chen YM, Xi TF, Zheng YF, Zhou L, Wan YZ, editors. In vitro structural changes of nano-bacterial cellulose immersed in phosphate buffer solution. *J Biomim Biomater Tissue Eng*; **2011**: Trans Tech Publ. https://doi.org/10.4028/www.scientific.net/JBBTE.10.55
66. Reddy MSB, Ponnamma D, Choudhary R, Sadasivuni KK. A comparative review of natural and synthetic biopolymer composite scaffolds. ***Polymers*** *(Basel)* **2021**; 13: 1105. https://doi.org/10.3390/polym13071105
67. 64. Stachurski ZH. On structure and properties of amorphous materials. *Materials* **2011**; 4: 1564-98. https://doi.org/10.3390/ma4091564
68. Kim J, Cai Z, Lee HS, Choi GS, Lee DH, Jo C. Preparation and characterization of a bacterial cellulose/chitosan composite for potential biomedical application. *Journal of Polymer Research* **2011**; 18: 739-44. https://doi.org/10.1007/s10965-010-9470-9
69. Gudkov SV, Burmistrov DE, Serov DA, Rebezov MB, Semenova AA, Lisitsyn AB. Do iron oxide nanoparticles have significant antibacterial properties? *Antibiotics* **2021**; 10: 884. https://doi.org/10.3390/antibiotics10070884
70. Pita-López ML, Fletes-Vargas G, Espinosa-Andrews H, Rodriguez-Rodriguez R. Physically cross-linked chitosan-based hydrogels for tissue engineering applications: A state-of-the-art review. *Eur Polym J* **2021**; 145: 110176. https://doi.org/10.1016/j.eurpolymj.2020.110176
71. Galateanu B, Bunea M-C, Stanescu P, Vasile E, Casarica A, Iovu H, *et al.* In vitro studies of bacterial cellulose and magnetic nanoparticles smart nanocomposites for efficient chronic wounds healing. ***Stem Cells*** *Int* **2015**; 2015. https://doi.org/10.1155/2015/195096
72. Viti F, Landini M, Mezzelani A, Petecchia L, Milanesi L, Scaglione S. Osteogenic differentiation of MSC through calcium signaling

activation: Transcriptomics and functional analysis. *PloS one* **2016**; 11: e0148173. https://doi.org/10.1371/journal.pone.0148173

73. Tanikake Y, Akahane M, Furukawa A, Tohma Y, Inagaki Y, Kira T, *et al.* Calcium concentration in culture medium as a nondestructive and rapid marker of osteogenesis. ***Cell** Transplant* **2017**; 26: 1067-76. https://doi.org/10.3727/096368916X694166
74. Chen J, Shi Z-D, Ji X, Morales J, Zhang J, Kaur N, *et al.* Enhanced osteogenesis of human mesenchymal stem cells by periodic heat shock in self-assembling peptide hydrogel. ***Tissue** Eng **Part** A* **2013**; 19: 716-28. https://doi.org/10.1089/ten.tea.2012.0070
75. Ressler A, Ródenas-Rochina J, Ivanković M, Ivanković H, Rogina A, Ferrer GG. Injectable chitosan-hydroxyapatite hydrogels promote the osteogenic differentiation of mesenchymal stem cells. *Carbohydr Polym* **2018**; 197: 469-77. https://doi.org/10.1016/j.carbpol.2018.06.029
76. Bayir E, Bilgi E, Hames EE, Sendemir A. Production of hydroxyapatite–bacterial cellulose composite scaffolds with enhanced pore diameters for bone tissue engineering applications. *Cellulose* **2019**; 26: 9803-17. https://doi.org/10.1007/s10570-019-02763-9
77. Zang S, Zhuo Q, Chang X, Qiu G, Wu Z, Yang G. Study of osteogenic differentiation of human adipose-derived stem cells (HASCs) on bacterial cellulose. *Carbohydr Polym* **2014**; 104: 158-65. https://doi.org/10.1016/j.carbpol.2014.01.019
78. Ma M, He W, Liu X, Zheng Y, Peng J, Xie Y, *et al.* Soybean protein isolate/chitosan composite microcarriers for expansion and osteogenic differentiation of stem cells. *Compos **B** Eng* **2022**; 230: 109533. https://doi.org/10.1016/j.compositesb.2021.109533
79. Menon AH, Soundarya SP, Sanjay V, Chandran SV, Balagangadharan K, Selvamurugan N. Sustained release of chrysin from chitosan-based scaffolds promotes mesenchymal stem cell proliferation and osteoblast differentiation. *Carbohydr Polym* **2018**; 195: 356-67. https://doi.org/10.1016/j.carbpol.2018.04.115
80. Marycz K, Sobierajska P, Wiglusz RJ, Idczak R, Nedelec J-M, Fal A, *et al.* Fe_3O_4 Magnetic Nanoparticles Under Static Magnetic Field Improve Osteogenesis via RUNX-2 and Inhibit Osteoclastogenesis by the Induction of Apoptosis. *Int J Nanomedicine* **2020**; 15: 10127. https://doi.org/10.2147/IJN.S256542
81. Lee S-C, Lee S-H, Kang D-H, Kim M, Sung J-S, Kadam AA. Supermagnetic α-cellulosic nano-scaffolds for human adipose-derived stem cells osteoconduction enhancement. *Cellulose* **2023**; 30: 2385-98. https://doi.org/10.1007/s10570-023-05045-7
82. Huang Z, Wu Z, Ma B, Yu L, He Y, Xu D, *et al.* Enhanced in vitro biocompatibility and osteogenesis of titanium substrates immobilized with dopamine-assisted superparamagnetic Fe_3O_4 nanoparticles for hBMSCs. *R Soc **Open** Sci* **2018**; 5: 172033. https://doi.org/10.1098/rsos.172033
83. Wang H, Zhao S, Zhou J, Zhu K, Cui X, Huang W, *et al.* Biocompatibility and osteogenic capacity of borosilicate bioactive glass scaffolds loaded with Fe3O4 magnetic nanoparticles. *J Mater Chem **B*** **2015**; 3: 4377-87. https://doi.org/10.1039/C5TB00062A